PERGAMON

Journal of Structural Geology 23 (2001) 1281–1298

JOURNAL OF STRUCTURAL GEOLOGY

www.elsevier.nl/locate/jstrugeo

Strain-insensitive preferred orientation of porphyroclasts in Mont Mary mylonites

Giorgio Pennacchioni[a,b,*], Giulio Di Toro[a], Neil S. Mancktelow[c]

[a]*Dipartimento di Geologia, Paleontologia e Geofisica, Università di Padova, Via Giotto 1, 35137 Padova, Italy*
[b]*CNR-Centro di Studi per la Geodinamica Alpina, Corso Garibaldi 37, 35137 Padova, Italy*
[c]*Geologisches Institut, ETH-Zentrum, CH-8092 Zurich, Switzerland*

Received 3 April 2000; revised 31 October 2000; accepted 27 November 2000

Abstract

The shape preferred orientation (SPO) of porphyroclasts was determined in high temperature mylonites. The porphyroclasts approach rhomboidal (sillimanite) or elliptical (garnet, plagioclase, sillimanite) shapes, and exhibit aspect ratios (R) as high as 11. Particles with $R > 3$ are dominantly rhomboidal. The long axis of the best-fit ellipse defines a very strong SPO inclined at 5–10° to the mylonitic foliation, in an antithetic sense with respect to the shear direction. This angle is independent of R. The inclination of the long sides of rhomboidal sillimanite increases from 10 to 20° with decreasing R. In contrast, the short sides have a constant orientation of 15 to 17° irrespective of R and are parallel to extensional crenulation cleavage. Low aspect ratio (mainly elliptical) objects show low intensity SPO close to the shear plane. The two SPOs appear strain-insensitive. In the case of $R < 3$, the SPO is caused by the combined effect of the slower rotation rate of elongate objects with long axes close to the shear plane and the continuous supply, by synkinematic fracturing and grain size refinement, of new porphyroclast populations. In the case of $R > 3$, a stable position is acquired. This is not explained by any of the current theoretical and experimental models of SPO.

1. Introduction

Mylonites are high strain rocks produced by localised ductile deformation. They are potentially an important source of information on the rheology and kinematics of flow occurring at depth in the crust and upper mantle. Apart from the use of fabric asymmetry as kinematic indicators, which is routine in modern structural studies, several microstructures of mylonites have been suggested as potential gauges for estimating deformation parameters (see Passchier and Trouw, 1996, for a review). In particular, porphyroclasts and porphyroclast systems could be sensitive indicators of rheology and/or vorticity. Synkinematic recrystallisation mantles around porphyroclasts develop characteristic σ- or δ-shaped tails whose geometry is at least in part dependent on the matrix rheology (Passchier and Sokoutis, 1993; Passchier et al., 1993; Bons et al., 1997; Pennacchioni et al., 2000). The shape preferred orientation (SPO) of porphyroclasts may also store information on the amount of shear strain (e.g. Fernandez et al., 1983) or the ratio between the pure and simple shear components of deformation (Passchier, 1987; Masuda et al., 1995).

Compared to the great effort invested in understanding the behaviour of porphyroclasts on a theoretical or experimental basis, relatively few studies have considered natural examples in rocks (Passchier, 1987; Hanmer, 1990; Masuda et al., 1995; Shelley, 1995). Consequently, it is not yet established if the behaviour of porphyroclasts in mylonites is well approximated by existing theoretical models and analogue experiments. The lack of a significant database is mainly due to the difficulty of finding rocks suitable for a statistical study and to the time-consuming task involved in measurement.

In this paper, the orientation of porphyroclasts in amphibolite facies mylonites of the Austroalpine Mont Mary nappe (Italian western Alps) is reported. The results are discussed and compared with the existing theoretical and experimental models of SPO. The comparison establishes that current models for rotation of rigid particles in isotropic media cannot explain the SPO observed in these natural mylonites. This implies that the SPO is controlled by rheological effects that are not yet considered in current theory or experiments.

* Corresponding author. Tel.: +390-49-827-2053; fax: +390-49-827-2070.
E-mail address: pengio@epidote.dmp.unipd.it (G. Pennacchioni).

0191-8141/01/$ - see front matter
PII: S0191-8141(00)00189-9

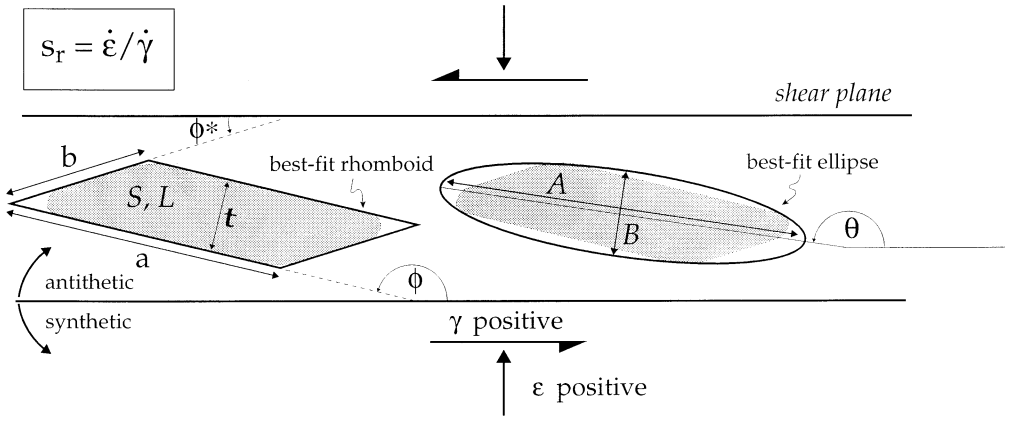

Fig. 1. Orientation and shape elements measured for rhomboidal *Sil* porphyroclasts. Positive angles are measured anticlockwise from the shear plane as indicated. Sinistral shear is taken as positive.

2. Motion of rigid objects in a viscous fluid

Based on Jeffery's (1922) theory, the equation of motion for an ellipsoidal rigid particle embedded in a viscous, incompressible fluid has been solved both analytically (Jeffery, 1922; Ghosh and Ramberg, 1976) and numerically (Hinch and Leal, 1979; Freeman, 1985; Ježek et al., 1994) for different low-Reynolds-number flow fields, over the range of 2D flows from simple to pure shear (Jeffery, 1922; Gay, 1968), and in 3D for axial flattening (Debat et al., 1975; Tullis, 1976) and general orthorhombic flow (Fernandez, 1988). Except for Ferguson (1979), analytical studies have considered only Newtonian linear–viscous fluids.

In 2D, the theoretical angular velocity ($\dot{\theta}$) of the long axis of an elliptical rigid particle is:

$$\dot{\theta} = \frac{1}{R^2+1}\left[\dot{\gamma}R^2\sin^2\theta + \dot{\gamma}\cos^2\theta - (R^2-1)\dot{\epsilon}\sin 2\theta\right] \quad (1)$$

(Ghosh and Ramberg, 1976), where R is the aspect ratio of the ellipse, and $\dot{\gamma}$ and $\dot{\epsilon}$ are the far field simple and pure shear strain rates, respectively (the angular and sign conventions are defined in Fig. 1). The relative components of pure and simple shear can be expressed as the ratio $s_r = \dot{\epsilon}/\dot{\gamma}$. Eq. (1) has the following implications:

1. A circular particle rotates with a constant angular velocity equal to $\dot{\gamma}/2$.
2. In simple shear ($s_r = 0$), an elliptical object always rotates but the angular velocity is pulsating and has a maximum when the long axis is perpendicular to the shear plane and a minimum when it is parallel. The shear strain necessary for a single complete revolution increases with increasing R.
3. In general, non-coaxial progressive deformation ($s_r \neq 0$), particles below a critical aspect ratio ($R_{crit} = \left(1 + \sqrt{4s_r^2 + 1}\right)/2s_r$) rotate with oscillating velocity, whereas more elongated particles approach a stable position inclined to the shear plane at an angle given by $90° \tan^{-1}\left(s_r(R^2-1) \pm \sqrt{s_r^2(R^2-1)^2 - R^2}\right)$ (Ghosh and Ramberg, 1976, eq. 8b; + sign for $s_r > 0$). The inclination is synthetic with regard to the shear component for a thinning shear zone ($\dot{\epsilon} > 0$) and antithetic for a thickening shear zone ($\dot{\epsilon} < 0$). The angle of inclination decreases with increasing R and s_r.

Many rock analogue experiments are in good agreement with the theoretical predictions (e.g. Robertson and Acrivos, 1970). In addition, these studies have allowed the behaviour of more complex particles than simple ellipsoids to be understood. 2D experiments in simple shear (e.g. Willis, 1977; ten Brink, 1996) indicate that the behaviour of orthorhombic particles is close to that of an ellipse with similar aspect ratio and that the exact shape of the particle has only a minor effect on its rotational behaviour. Experiments by Arbaret et al. (2001) establish that the 2D simplification of previous experiments is also valid in 3D. As part of the same study, monoclinic particles with an aspect ratio up to ~4 were investigated. Such particles still rotate continuously, though with variable angular velocity, under simple shear and for a Newtonian linear–viscous matrix. These experimental results can be directly compared with our natural observations.

3. Theoretical and experimental models of preferred orientation of porphyroclasts

In a flowing matrix, a SPO of embedded rigid particles can develop during magmatic (e.g. Benn and Allard, 1989; Luneau and Cruden, 1998), cataclastic (Cladouhos, 1999a) and mylonitic deformation (e.g. Passchier, 1987; Hanmer, 1990; Shelley, 1995; Masuda et al., 1995). Several models, based on experimental data or theoretical analysis, have been proposed to account for the development of SPO in rigid objects undergoing non-coaxial flow in a viscous matrix (Table 1).

Jeffery's theory for the rotational properties of individual

Table 1
Existing models for development of SPO in a population of rigid particles

Model	Model type	Model characteristics	Fabric stability	Fabric intensity	Fabric orientation
1	Theoretical (Ghosh and Ramberg, 1976)	Non-interacting particles (simple shear)	Transient	Zero to high (higher with increasing aspect ratio)	Symmetric at the maximum intensity
2a (thinning), 2b (thickening)	Theoretical (Ghosh and Ramberg, 1976)	Non-interacting particles (general non-coaxial flow)	(i) Transient ($R < R_{crit}$) (ii) Stable ($R > R_{crit}$)	(i) Zero to high (ii) Very high (approaching perfect parallelism)	(i) Symmetric (ii) Asymmetric (synthetic for 2a, antithetic for 2b)
3	Theoretical (Luneau and Cruden, 1998)	Non-interacting particles with continuous addition of new populations (simple shear)	Strain insensitive	Low	Symmetric
4	Experimental (Ildefonse et al., 1992a,b)	Interacting particles in high-concentration suspension (simple shear)	Strain insensitive	Low	Bimodal (symmetric and antithetic asymmetric)
5	Experimental (Arbaret et al., 1996)	Interacting particles in low-concentration suspension (simple shear)	(i) Transient (low strains) (ii) Strain insensitive (high strains)	Low	(i) Indeterminate (ii) Antithetic asymmetric
6	Numerical (Tikoff and Teyssier, 1994)	Particle interaction and rotation of trains of tiled particles according to the Jeffery theory (simple shear)	Effectively strain insensitive	Low	Antithetic asymmetric
7	Experimental (Ildefonse and Mancktelow, 1993)	Slip at particle/matrix interface, power law rheology (simple shear)	Strain insensitive? (final shear strain too low to be established)	Low	Antithetic asymmetric
8	Theoretical (Cladouhos, 1999b)	Matrix deformation by concomitant particulate flow, synthetic and antithetic Riedel shears	Strain insensitive	Low	Antithetic asymmetric

particles can be used to predict the development of SPO (Reed and Tryggvason, 1974; Willis, 1977; Passchier, 1987; Ježek et al., 1994; Masuda et al., 1995). For originally randomly oriented non-interfering objects in a matrix deforming by simple shear, elongated porphyroclasts develop a statistical SPO close to the shear plane for specific values of the shear strain and aspect ratio. Model 1 predicts that the SPO is transient and oscillating, periodically strengthening and weakening during progressive deformation. Since both the maximum strength of the SPO and the strain necessary for a single cycle increases with increasing aspect ratio of the particles, the long axes of high aspect ratio particles can remain close to the shear plane for quite large γ values, which may give rise to apparently strain-insensitive fabrics.

In the case of a general non-coaxial deformation ($s_r \neq 0$), Model 2 predicts the development of a composite fabric for non-interacting particles with different aspect ratio. For particles with aspect ratios below the critical value, a transient SPO develops (similar to Model 1), whereas a strong strain-insensitive asymmetric SPO develops for particles exceeding R_{crit}, by stabilisation at a sink position determined by R and s_r. If the SPO of porphyroclasts follows this model, then it may be used to infer the kinematic vorticity number of deformation in mylonites (Passchier, 1987; Masuda et al., 1995). The angle of inclination of this stable SPO to the shear plane decreases as R increases. The orientation with regard to the shear sense is synthetic for thinning (Model 2a) and antithetic for thickening (Model 2b) shear zones.

Both the above models assume stable shapes and/or a constant number of porphyroclasts, no interference between objects, and perfect coupling at the matrix/particle interface. These assumptions are seldom strictly correct for real rocks. The effect of adding new populations of rigid objects with a random orientation during deformation was modelled by Luneau and Cruden (1998) (Model 3). They applied the model to magmatic fabrics, where reorientation of 'old' grains may occur during concurrent crystallisation of new ones. The resulting fabric is strain-insensitive and symmetric, with a peak in the orientation parallel to the shear plane. Because it is a cumulative fabric, the SPO is weaker than for Model 2.

In dense suspensions, particle interaction has important consequences for the development of SPO and may lead to a steady-state SPO for very high simple shear produced strain values (Mason and Manley, 1957). In 2D simple shear experiments at finite strain up to 9, Ildefonse et al. (1992a,b) observed a slowing down of particle rotation. Owing to interaction, the fabric evolution for elongated particles is no longer cyclic. The fabric intensity is on average weaker than for isolated particles and the fabric rotates asymptotically toward the shear plane (Model 4).

Even in low-concentration suspensions, particle interference may become important at large shear strain, owing to the increased possibility of interaction between particles to form tiled aggregates (Arbaret et al., 1996). In the simple shear experiments of Arbaret et al. (1996), the rotational behaviour of rectangular objects in low-concentration suspension (13–14% in area) evolves according to the theoretical models for $\gamma < 6$. For larger shear strains, particle interaction affects the SPO (Model 5) in a similar way to that described above for high concentration suspensions (Model 4). The shape fabric becomes asymmetric, with a SPO antithetic to the shear plane. The cyclicity practically disappears, but the intensity remains low.

Tikoff and Teyssier (1994) proposed three 2D-computer models for the development of SPO in aggregates with interacting low-ellipticity particles. The models differ in the assumed kinematic behaviour of isolated particles and trains of tiled particles: (i) trains are fixed and isolated clasts rotate as passive lines according to the March (1932) model; (ii) both trains and clasts rotate according to the March model; and (iii) isolated particles and trains rotate according to the Jeffery theory. In (ii) and (iii), particles are released from the tiled trains when they are no longer forced together by the flow. The Jeffery model gives results comparable with Models 4 and 5. The two March models give rise to a more intense SPO, still inclined to the shear plane. In Table 1, only the Jeffery model is considered (Model 6), since use of the March theory, which assumes the particles rotate as passive lines (or infinitely elongated particles), is highly questionable.

The effect of slip at the particle/matrix interface for isolated rectangular particles in a matrix with power-law rheology has been studied by Ildefonse and Mancktelow (1993). In simple shear experiments, particles rotate more slowly and develop a SPO more rapidly than for non-slip. The SPO tends to be bimodal, with one set of particles oriented sub-parallel to the shear plane at high shear strains and the other set at about 30° to the shear plane (Model 7). Unfortunately, the experimental runs were limited by machine constraints to $\gamma \leq 3$.

Cladouhos (1999a,b) developed a kinematic model to interpret the observed preferred orientation of clasts in a fault gouge. Since the model is purely kinematic, it is independent of any assumed rheology and could equally well be applied to ductile shear zones. The model is based on the observation of concomitant activity, during fault gouge deformation, of three different modes: synthetic Riedel shear (R_1), antithetic Riedel shears (R_2) and shearing particulate flow (P). This model predicts different SPO depending on the relative shear activity along P, R_1 and R_2. In the case of a P–R_1 composite fabric, the model can explain a strong SPO for clasts with a maximum inclined at a low antithetic angle to the shear plane (Model 8). Kinematically, the model is identical to that proposed by Mancktelow (1987) for the development of a stable crystallographic preferred orientation in quartz mylonites by concomitant synthetic slip on two easy glide planes during crystal–plastic deformation.

4. Study of preferred orientation of porphyroclasts in the Mont Mary mylonites

The studied mylonites are from the Austroalpine Mont Mary (MM) unit of the Italian western Alps, described in Pennacchioni and Cesare (1997). This unit represents a slice of pre-Alpine continental lower crust involved in the Alpine orogeny. The mylonites developed from upper amphibolite facies metapelites (*Bt*, *Grt*, *Sil*, *Kf*, *Pl*)[1] during deformation at 510–580°C and 0.25–0.45 GPa, under water-deficient conditions (Pennacchioni and Cesare, 1997). The mylonites consist of a matrix (average grain size of 1–5 μm) of *Bt* with additional *Ilm*, *Qtz*, *Ms* and *Gph*, including numerous porphyroclasts of *Grt*, *Pl* and *Sil* (Fig. 2). Most ultramylonites display a fine composite foliation made up of three planar subfabrics.

1. A compositional layering/foliation, subparallel to the shear plane, is the dominant feature (Fig. 2).
2. A transverse foliation, inclined at an antithetic angle ≤45° with respect to (1), is defined by a SPO of finely granulated *Ilm* in mica-rich layers or of *Qtz* grains in dynamically recrystallised aggregates.
3. A discontinuous, finely spaced (on the scale of 10s to 100s of microns) extensional crenulation cleavage (ECC, e.g. Platt and Vissers, 1980) inclined at a synthetic angle of ~20° to the shear plane. The ECC is evident and pervasive in some thin sections but only very faintly developed in others. The ECC is generally confined to mica-rich layers and often nucleates (or is pinned) on opposite sides of porphyroclasts.

The MM mylonites were selected for this study of preferred orientation of porphyroclasts for several reasons: (1) porphyroclasts are abundant up to high shear strains; (2) differently shaped porphyroclasts, with a large range in particle aspect ratio, are available; (3) porphyroclasts commonly approach either perfectly elliptical or rhomboidal shapes and are, therefore, comparable with shapes used in experiments; and (4) the matrix has an ultrafine grain size, so that the distinction between 'porphyroclasts' and 'matrix' is clear.

5. Porphyroclast shape

Pl and *Grt* porphyroclasts are commonly well rounded, elliptical to circular grains (Fig. 3a). Rare elongated *Grt* clasts have a rhomboidal shape similar to *Sil*. *Grt* porphyroclasts are surrounded by asymmetric *Bt* appendages resembling σ- to (less commonly) δ-shaped porphyroclast systems. *Grt* porphyroclasts develop by extensive cataclasis or domino-style, antithetic microfaulting of coarse *Grt* porphyroblasts (Fig. 3b). Mixed microcataclasis and reaction to *Bt* during rotation produce a smoothing and rounding of clasts to regular circular and elliptical shapes from precursor equant and elongated grains, respectively. Pervasive cataclasis, by a network of interfering conjugate fractures, produces approximately equant grains with irregular shape, while domino microfaulting gives rise to elongated clasts with parallel long sides. Fracturing occurs episodically, possibly caused by impact between porphyroclasts of similar size. Fractures are sealed with *Bt* aggregates, which assist the relative displacement of *Grt* fragments with increasing strain. The *Grt* site is thereby deformed to roughly elliptical *Bt–Grt* domains. Low aspect ratio *Bt–Grt* domains are inclined at angles close to 45° to the mylonitic foliation and *Grt* clasts are densely packed. With increasing aspect ratio, the angle of inclination decreases and *Grt* clasts become increasingly separated in the *Bt* matrix (Figs. 2 and 3c). *Grt* clasts in *Bt–Grt* domains are angular, in contrast to isolated small *Grt* clasts in the matrix, which are usually well rounded and elliptical to circular. Both the progressive decrease in the angle of inclination of *Bt–Grt* domains and the separation of clasts provide a potential estimate of strain, as discussed below.

Pl porphyroclasts are produced by the disruption of initial millimetre-sized grains by microshearing and fracturing. Isolated porphyroclasts in the matrix are commonly perfectly elliptical to circular in form and show mantles of recrystallised ultra-fine-grained *Pl* aggregates. The recrystallised mantles are strung out to form δ- or complex-shaped wings (Fig. 3a).

Sil porphyroclasts have a variety of shapes: rectangular, rhomboidal and elliptical (Fig. 3d). Rectangular *Sil* occurs in low-strain domains and in protomylonites and is derived from microboudinage of coarse-grained *Sil* common in the protolith. Rhomboidal and elliptical *Sil* are typical of mylonite/ultramylonites and clearly derive from previous rectangular *Sil* microboudins. Rhomboidal grains are the most frequent. Their shape varies from true rhombs (orthorhombic symmetry) to highly asymmetric rhomboids (monoclinic symmetry), with the long sides parallel to the {010} cleavage. Where visible in the mylonitic matrix, ECC planes are always tangential to the short sides of *Sil* rhomboids (Fig. 4a). In detail, deviation from ideal rhomboidal shape is caused by rounded corners and/or curved short sides, giving the porphyroclasts the aspect of a sigmoidal mica-fish (but with the opposite asymmetry in shape for the same shear sense; Fig. 3d), or to incomplete development of the short rhomboidal sides, associated with additional short rectangular faces orthogonal to the {010} cleavage (Fig. 4b). *Sil* has locally thin mica appendages extending straight into the foliation and stair-stepping from the tips of rhomboidal clasts, or deformed into δ-shaped tails around elliptical clasts.

Sil rhomboids are commonly present in associations of two or more tiled crystals (e.g. Fig. 4a). In samples with evident ECC, tiled particles are frequent and adjacent ECC

[1] The following mineral abbreviations are used in the text: *Bt* = biotite, *Pl* = plagioclase, *Qtz* = quartz, *Gph* = graphite, *Grt* = garnet, *Ilm* = ilmenite, *Kf* = K-feldspar, *Ms* = muscovite.

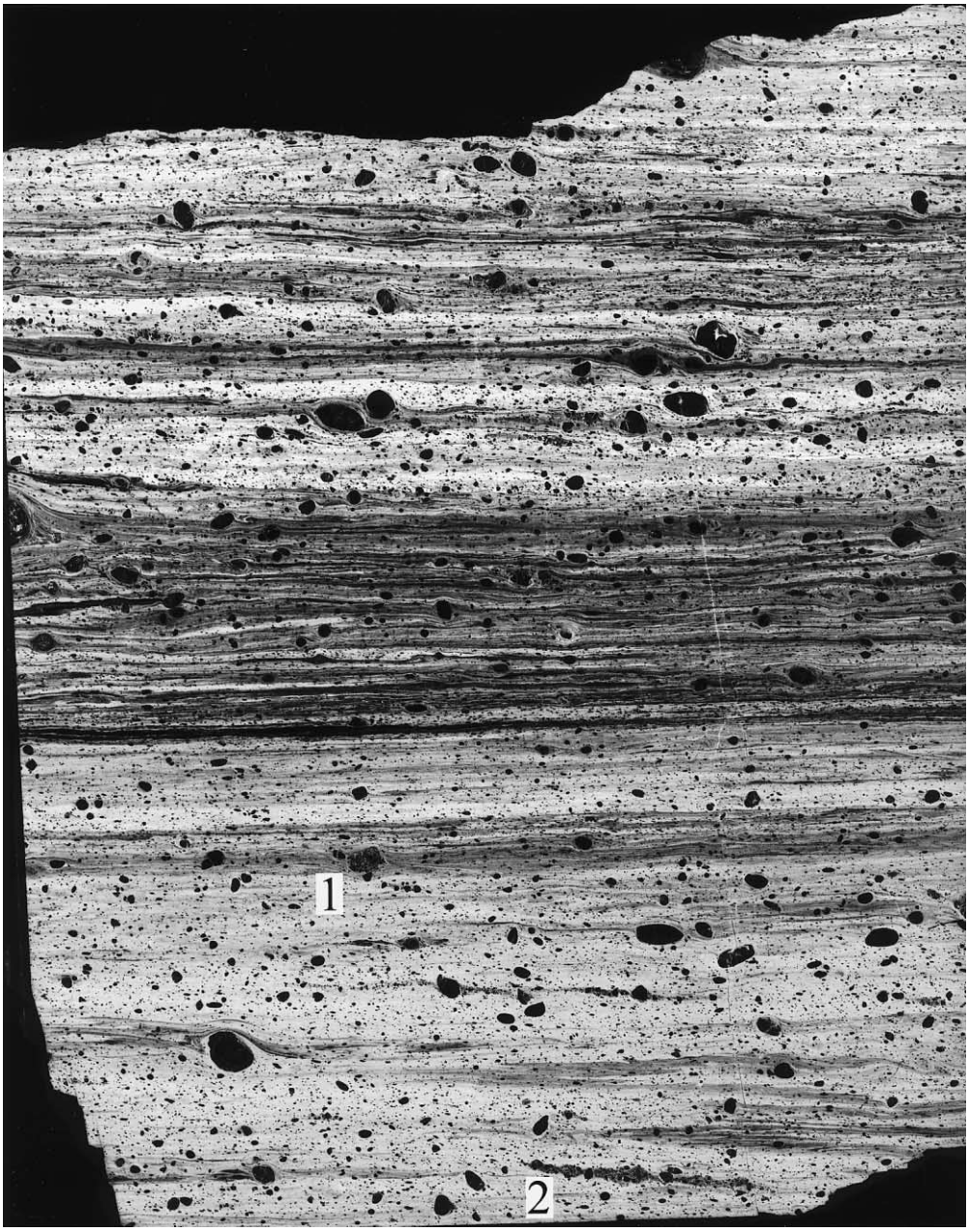

Fig. 2. Negative print of a 2.7 × 3.8 cm thin section of the sample 06. The fine-grained, *Bt*-dominated matrix, derived from recrystallisation of the protolith *Bt*, is white to light grey (it has in fact a turbid appearance in thin section under crossed polars because of finely granulated *Ilm*). Darker grey matrix layers are mainly *Bt*-rich matrix (free of *Ilm*) derived from transformation of *Grt*, whereas thin black layers are dynamically recrystallised *Qtz* ribbons. *Grt*, *Pl* and *Sil* porphyroclasts are black. The largest porphyroclasts are *Grt* and *Pl*; they are smaller than porphyroblasts in the undeformed protolith and, therefore, already represent porphyroclasts. Some of these are extensively fractured but still 'undeformed' (1), whereas others have flowed to elongated *Grt–Bt* domains inclined at a low angle to the mylonitic foliation (2). Sense-of-shear is sinistral. Plane of view is perpendicular to the foliation and contains the lineation (*XZ* section).

planes often include several tiled grains. During deformation, porphyroclasts of *Sil* undergo episodic microboudinage along fractures almost orthogonal to the long axis (Fig. 4c and d). Fracturing mainly occurs when *Sil* interacts with *Grt* and *Pl* porphyroclasts (Fig. 4c) that have grain diameters in the same range as the length of the *Sil*. Crystal–plastic effects are never observed in *Sil*.

In thin sections orthogonal to the mylonitic foliation and parallel to the lineation (*XZ* section), rhomboidal *Sil* are the most common (Fig. 4e) and show homogeneous high interference colours. In contrast, some elliptical grains show rather low interference colours, suggesting that the difference in shape is, at least in part, crystallographically controlled. In thin sections orthogonal to the mylonitic foliation and lineation (*YZ* section), rhomboidal/elongated *Sil* are rare and *Sil* is mainly represented by equant, approximately idioblastic, basal sections (Fig. 4f) with very low interference colours. This indicates that rhomboidal *Sil*

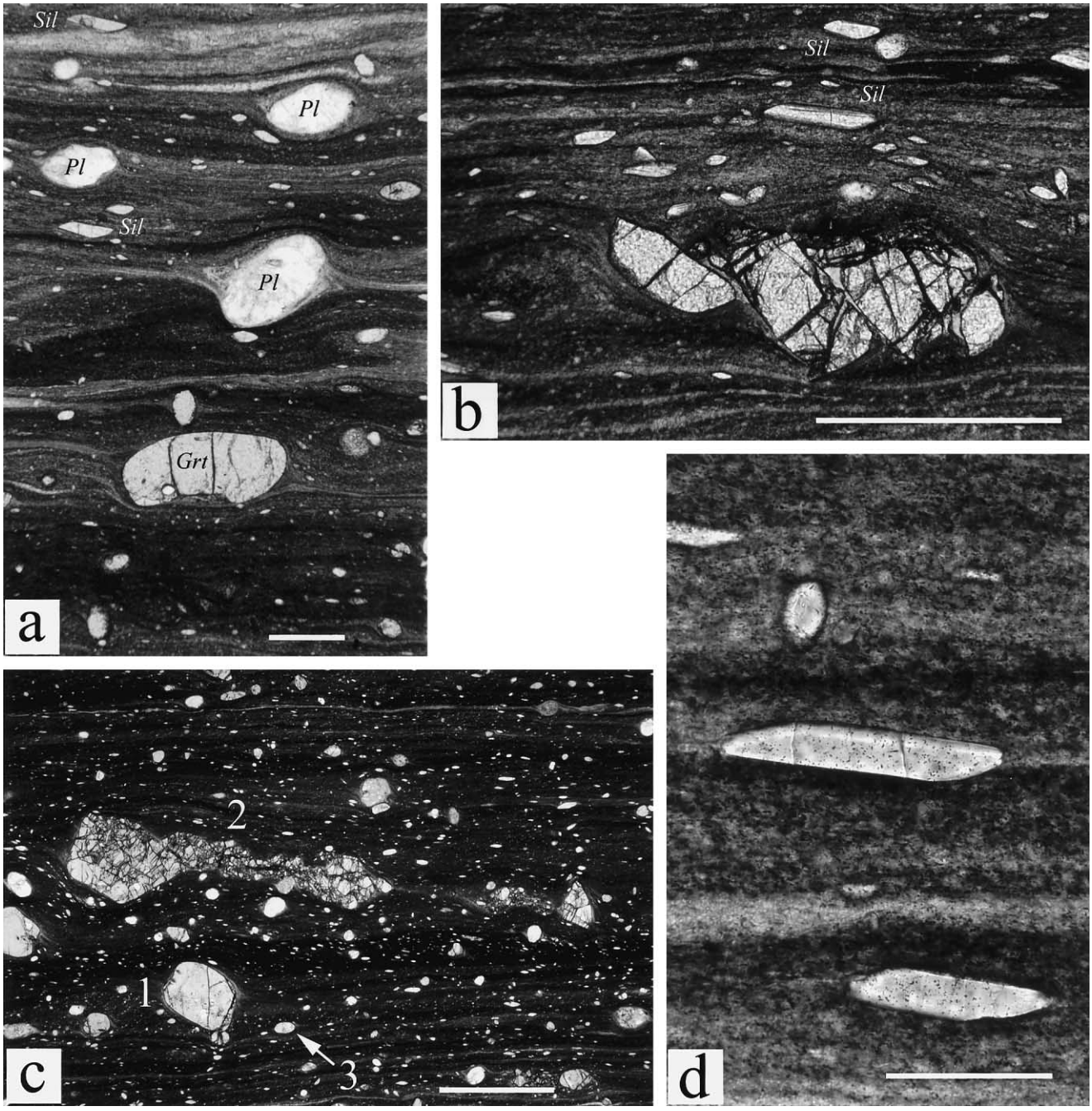

Fig. 3. Microstructures in MM mylonites. (a) Well grain-size-refined, elliptical *Grt* and *Pl* porphyroclasts (in some cases with complex tail geometry) and rhomboidal *Sil*. (b) Domino-style antithetic fracturing of a *Grt* porphyroclast. (c) Coexisting unbroken *Grt* (1) and cataclastic elongated *Grt* (+*Bt*) aggregate (2) with the long axis making a low angle with the mylonitic foliation. In the aggregate, clasts are irregular/angular, while isolated small porphyroclasts in the matrix commonly show well-refined elliptical/circular shapes (3). (d) Stair-stepping rhomboidal high aspect ratio *Sil* and low aspect ratio elliptical *Sil*. Sense-of-shear is sinistral in all photographs. Plane polarised light. *XZ* section. Scale bar is 200 μm in (a), 500 μm in (b), 1 mm in (c) and 100 μm in (d).

porphyroclasts have a strong nearly uniaxial SPO oriented close to the mylonitic foliation and within the *XZ* section.

6. Measurements

Two mylonites (samples 03C and 06) were selected for measurement. Observations were made on thin sections cut orthogonal to the mylonitic foliation and parallel to the stretching lineation (*XZ* section). Most of the measurements were taken from sample 06, which was serially cut to obtain 16 thin sections (889 *Sil*, 433 *Grt*, 163 *Pl*). In addition, five thin sections of sample 03C were studied (352 *Sil*, 112 *Grt*). In hand specimens, both samples have a strong foliated-lineated fabric. As in the sample presented as Fig. 2b in Pennacchioni and Cesare (1997), the two samples contain

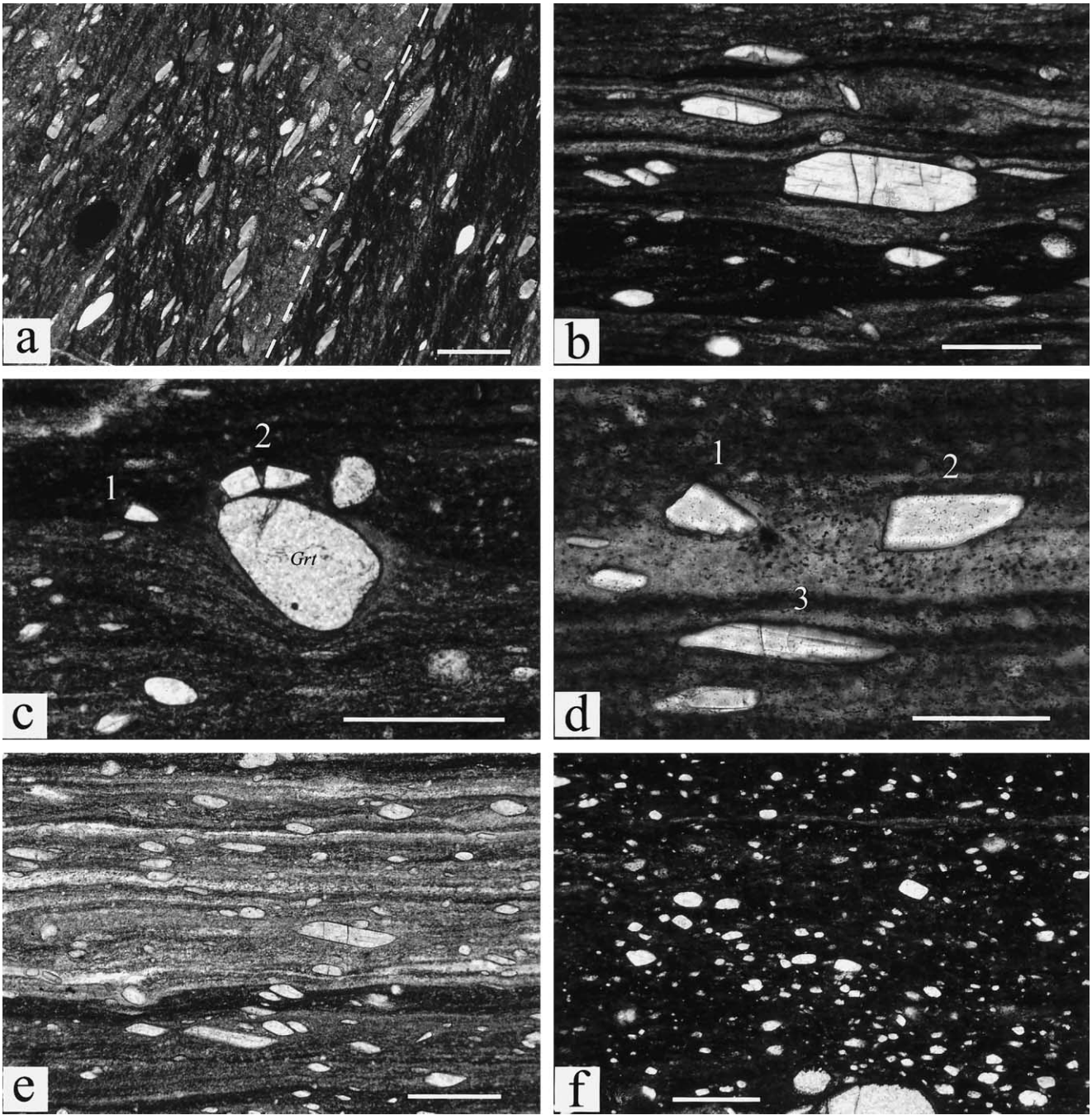

Fig. 4. Microstructures in MM mylonites. (a) Closely-spaced ECC-surfaces inclined at a low angle to the mylonitic foliation (dashed) and making a tangent to the *b*-sides of well-oriented *Sil* rhomboidal porphyroclasts. (b) Different shapes of rhomboidal *Sil*. The largest central porphyroclast has composite short faces with rectangular and rhomboidal sides. Long faces develop parallel to {010} cleavage in *Sil*. Above the central large *Sil*, two porphyroclasts show the transition from rhomboidal to sigmoidal shapes. Note the train of three tiled particles (left central position) with an orientation similar to the isolated rhomboidal *Sil*. (c) Fracturing of *Sil* interfering with a *Grt* porphyroclast. One *Sil* fragment (1) has clearly rotated and flowed away from the other clasts (2). (d) Rotated portions of a fragmented *Sil* porphyroclast; the fragment with lower aspect ratio (1) has clearly rotated more than the other higher aspect ratio fragment (2). In both cases, the clast aspect ratio is less than three. Below, the elongated ($R > 3$) rhomboidal *Sil* porphyroclast (3) makes a low antithetic angle with the foliation. (e) Rhomboidal *Sil* with a strong SPO (note the tiled particles in the central bottom part of the photo). (f) Equant, idioblastic basal shapes of *Sil* porphyroclasts typical of thin sections orthogonal to the mylonitic lineation. For (a)–(e), sense-of-shear is sinistral and view is an *XZ* section. View is a *YZ* section for (f). Scale bar is 100 μm in (d) and 200 μm in the other photographs.

transitions from mylonitic (richer in macroscopic porphyroclasts and coarser fabric) to dominantly ultramylonitic domains (characterised by an extremely fine, regular 'varved-like' layering and a scarcity of macroscopic porphyroclasts). Thin section analysis supports the existence of corresponding strain gradients between adjacent domains, as revealed by different degrees of fabric refinement. The overall degree of grain size refinement,

the size, density and aspect ratio distribution of porphyroclasts, the occurrence of non-recrystallised relicts of *Qtz* and *Bt* mica-fish and other fabric characteristics allow a rough qualitative estimate of the strain magnitude. The main microscopic difference between the two samples is the occurrence of a pervasive fine ECC in the mica-rich matrix of sample 03C, which is only faintly developed in sample 06. In sample 03C, ECC is evident as planes extending far away from individual porphyroclasts (i.e. several times the dimensions of the porphyroclast) whereas, in sample 06, they are visible only at high magnification and are commonly short and merge into the mylonitic foliation very close to the porphyroclast. Overall, sample 03C also contains a higher density of porphyroclasts than does sample 06.

The first set of measurements considered isolated (i.e. not in close proximity to other porphyroclasts of comparable dimensions), nearly elliptical or rhomboidal porphyroclasts, in regions of undisturbed planar foliation. In a second set of measurements, all *Sil* porphyroclasts in different areas of undisturbed, straight foliation were measured to check for any influence of porphyroclast interference, since many porphyroclasts do show visual evidence of tiling (e.g. Fig. 4b and e). All analysed grains were recorded on enlarged photographs to avoid measuring the same grain twice. Measurements were made using image analysis software (NIH image) on a computer connected to the microscope via a video camera. Images were captured at the largest possible enlargement to reveal shape details.

The orientation, sign convention and enveloping shape elements used in measuring the porphyroclasts are given in Fig. 1. The following data were collected: the length of the long (A) and short (B) axis of the best-fit ellipse, its ellipticity (R) and inclination (θ), the area (S) and perimeter (L) of the grains. In addition, for rhomboidal *Sil*, the thickness (t), the length of the long and short sides (a and b) and their inclinations (ϕ and ϕ^*) of the 'best-fit rhomboid' were measured.

7. Results

7.1. Aspect ratio of porphyroclasts

Grt, *Pl* and *Sil* show a different range in the aspect ratio of the best-fit ellipsoid. Aspect ratios (R) are generally less than three for *Grt* and less than two for *Pl*, with only a few percent of porphyroclasts exceeding these values. With regard to *Sil*, rhomboidal shapes have R as high as 11 and commonly higher than three, whereas elliptical shapes are characterised by R commonly in the range between two and three, similar to *Grt*. The highest shape ratios of *Sil* are found in sample 03C, which also shows a higher density of porphyroclasts and a lower overall degree of fabric evolution than sample 06.

7.2. Shape preferred orientation

The orientations of the long axis of the best-fit enveloping ellipse (θ) of porphyroclasts are plotted, as a function of the particle aspect ratio, in Fig. 5. The orientation and intensity of the SPO may be quantitatively estimated by computing the *semicircular vector mean* ($\hat{\mathbf{V}}$) and the *vector mean strength* ($\bar{a}$) (e.g. Agterberg, 1974; Cladouhos, 1999a). The values of $\hat{\mathbf{V}}$ and $\bar{a}$ for the best-fit ellipse are given, for different ranges in aspect ratio, in Table 2 and plotted in Fig. 6. The magnitude of the vector mean strength $\bar{a}$ varies from zero, for a perfectly uniform distribution, to one for a population of parallel lines.

Analysis of the data demonstrates that, except for very low aspect ratios, *Sil*, *Grt* and *Pl* all have a significant SPO. The SPO has a variable intensity depending on the aspect ratio of porphyroclasts. In all cases, however, (i.e. over the whole range of R and in both samples), the mylonites show a SPO of porphyroclasts close to the shear plane with a mean vector oriented within $\pm 10°$ of the mylonitic foliation. The only exceptions are for very low aspect ratio particles, which approach a random fabric and for which the resulting SPO has no real statistical meaning. To a first approximation, there is a consistent behaviour of *Pl*, *Grt* and elliptical *Sil* for the same range of aspect ratios. In addition, the effect of shape on the SPO appears to be negligible, since both elliptical and rhomboidal objects develop SPOs with similar fabric intensities and orientations for similar aspect ratios.

In sample 06, two types of SPO are clearly distinguishable, which develop above and below a critical aspect ratio value of ~ 3.

1. For $R > \sim 3$, the value of R has practically no influence on the fabric intensity and orientation. The porphyroclast long axes are nearly perfectly parallel ($\bar{a} > 0.97$) and define a transverse SPO oriented at a low antithetic angle to the mylonitic foliation ($\hat{\mathbf{V}} = \sim -6°$). This preferred orientation is evident to the eye in thin section and is present in all samples of MM mylonites (currently more than 100). This means that the tips of rhomboidal *Sil* porphyroclasts show a stair-stepping asymmetry similar to that commonly shown in mylonites by mica-fish. The same attitude is also shown by elliptical *Sil*, *Grt* and *Pl* porphyroclasts.
2. For $R < \sim 3$, the fabric intensity is strongly influenced by the aspect ratio and becomes weaker as R decreases. Porphyroclasts are preferentially oriented with the long axis close to the shear plane, but the presence of SPO can no longer be recognised from simple visual inspection. The calculated fabric orientation and intensity must be considered as a semiquantitative estimate of the SPO, since the number of analysed particles for any R range is relatively small considering the dispersion of the data.

Data from sample 03C are comparable with those of sample 06 with two main differences: in 03C a strong

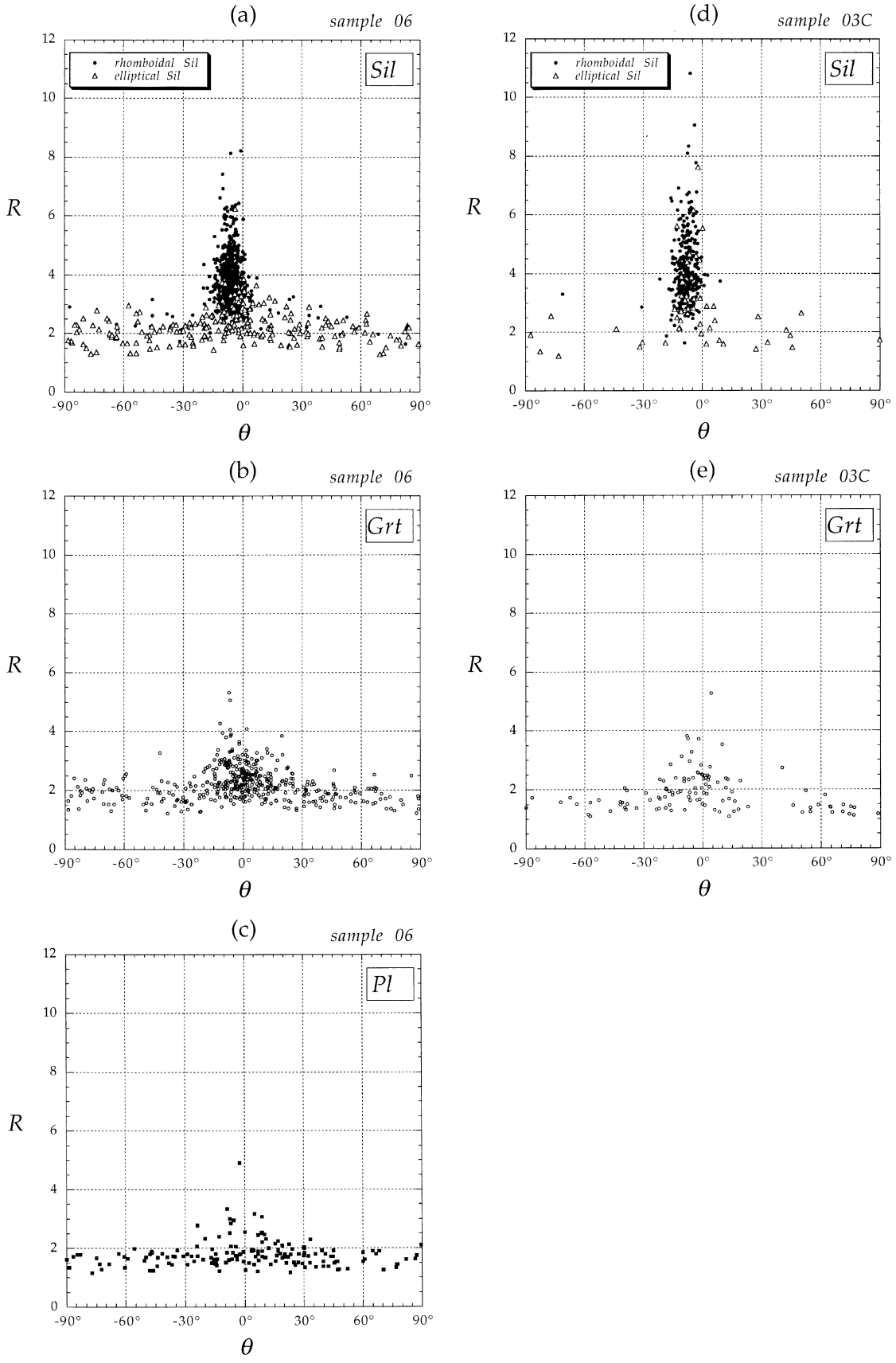

Fig. 5. The orientations (θ) of porphyroclasts plotted as a function of the particle aspect ratio R. The left column is for sample 06 (a for *Sil*, b for *Grt*, c for *Pl*), the right column for sample 03C (d for *Sil*, e for *Grt*). Note that the preferred orientation of high aspect ratio *Sil* is independent of R; note also the consistency both between different samples and between different porphyroclasts with similar aspect ratio.

($\bar{a} > 0.95$) *R*-insensitive SPO is also found for isolated *Sil* even when *R* is less than three, and the SPO fabric is oriented at a slightly higher angle to the shear plane ($\hat{\mathbf{V}}$ in the range of -7 to $-9°$).

Data on isolated *Sil* (*rhomboidal* and *elliptical Sil* in Fig. 6 and Table 2) are consistent with those for orientations of total *Sil* porphyroclasts from small sample areas (reported as *Sil area* in Fig. 6 and Table 2). In the small areas considered, high aspect ratios are not common, but their orientation is consistent with data on isolated particles. In sample 03C, the overlap between the orientation of isolated porphyroclasts and of total porphyroclasts is particularly striking (Fig. 6b). In fact, to a first approximation, interfering *Sil* porphyroclasts (tiles) have orientations similar to isolated particles and any tiling effects, such as were found in the experiments of Arbaret et al. (1996), are not observed. In MM mylonites, tiled particles maintain their stair-stepping orientation despite coupling.

In contrast to θ (the orientation of the best-fit ellipse long axis), which is not affected by the particle aspect ratio for $R > 3$, the inclinations ϕ of the long side of rhomboidal *Sil* is a function of *R* (Fig. 7). This effect is evident in both samples. The angle that the mean vector for ϕ makes with the shear direction changes from values in the range of -9 to $-10°$ for particles with $R > 6$ to values in the range of -14 to $-16°$ for $R = 3$–4 (Table 3). The fabric intensity is always high ($\bar{a} > 0.98$). A further decrease in particle aspect ratio ($R = 2.5$–3) consistently results in a further change of the ϕ mean vector to values in the range of -18 to $-19°$. It is remarkable, however, that the fabric intensity, even if somewhat reduced in sample 06, still remains high.

The inclination of the mean vector of ϕ^* for the short sides of high aspect ratio (i.e. $R > 3$) rhomboidal *Sil* has a constant orientation of 15–17° independent of *R* (Fig. 8) and identical for the two samples. The fabric intensity is consistently very high ($\bar{a} > 0.97$, Table 4). This is despite the fact that there is some data dispersion induced by the roundness of the *Sil* short sides, making it difficult to exactly determine the orientation of the *b* sides at times. As in the case of ϕ, in the range $R = 2.5$–3, the vector mean of ϕ^* is almost identical for the two samples but has a decreased intensity in sample 06. In sample 03C, it is very clear from visual inspection that the short sides of the rhomboidal *Sil* clasts are tangential to ECC planes (Fig. 4a).

8. Discussion

8.1. Estimate of the shear strain experienced by the porphyroclasts

Understanding the strain history undergone by the porphyroclasts in the MM mylonites is crucial for any interpretation of the SPO. This is particularly true when considering whether the fabrics are strain-insensitive, because the magnitude of the shear strain may be insufficient to establish the true rotational behaviour of porphyroclasts. In most thin sections of MM mylonites, it is clear that porphyroclasts have experienced different amounts of total strain, because they were produced at different times during increasing deformation. In the same thin section, deformed *Grt–Bt* domains, derived from cataclasis and displacement of former *Grt* porphyroblasts, show different aspect ratios and inclinations to the shear plane. It is assumed that these domains have the form of the strain ellipse and record the amount of strain since the time of fracturing. Low-aspect-ratio domains, inclined ~45° to the foliation, suggest near simple shear bulk flow (see e.g. Ramsay and Huber, 1987). With increasing γ, the *Grt–Bt* domains are rotated towards the shear plane and increase in aspect ratio. Concomitantly, *Grt* clasts are progressively separated, resulting in a decrease in the *Grt*/*Bt* ratio. Assuming simple shear, the very low inclination, high-aspect-ratio *Grt–Bt* domains, in which *Grt* clasts are still densely clustered, require shear strains on the order of 15–20. With further strain, the domains are effectively transposed into the foliation and *Grt* clasts are progressively separated, become more rounded, and finally occur as small porphyroclasts isolated in the matrix. These rounded porphyroclasts, comparable in size with clasts in the *Grt–Bt* domains, are clearly produced during synmylonitic deformation, because such small grains are not present in the protolith. Evolution to regular rounded elliptical shapes, typical of isolated small grains, requires quite high strains ($\gamma \gg 20$) since the *Bt–Grt* aggregates, transposed in the foliation but still showing closely-spaced clusters of *Grt* clasts ($\gamma \sim 15$–20), only exhibit a low degree of grain shape refinement of clasts. It follows that different *Grt* porphyroclasts have experienced a wide range of strain, increasing from the most recently developed fragments in highly inclined, low-aspect-ratio domains, to isolated small well-refined porphyroclasts, to relict protolith *Grt* porphyroblasts that have experienced the total finite strain in the mylonites.

A similar genetic history can be suggested for *Sil* porphyroclasts, whose aspect ratio is progressively diminished by microboudinage/fracturing. Even in the case of a constant or relaxing bulk differential stress, which theoretically would stop fracturing of isolated clasts (Masuda et al., 1990), fracturing remains frequent because of impacting between porphyroclasts.

In summary, porphyroclasts are produced from episodic but continuous fragmentation. Clasts produced late in the history of the mylonitic deformation experienced only relatively small strains but coexist with relicts and clasts produced during initial deformation, which have experienced the total (and high) bulk deformation. Therefore, in MM mylonites, the SPO is caused by the orientation of clasts that have undergone very different amounts of strain (strain telescoping). In addition, the microstructural characteristics of the mylonites indicate that the total accumulated shear strains are high ($\gg 20$). It follows that the development of a strong transverse SPO of elongated *Sil*,

Table 2
SPO intensity and orientation for θ of the best-fit ellipse (see Fig. 1), expressed as *semicircular vector mean* ($\hat{\mathbf{V}}$) and the *vector mean strength* ($\bar{a}$), calculated for different aspect ratios R in sample 06 (a) and sample 03C (b). # is the number of particles for each aspect ratio range. Data refer to isolated porphyroclasts or, in the case of *Sil area*, to the total particles present in small sample areas

Rhomboidal Sil				*Elliptical Sil*				*Sil area*				*Grt*				*Pl*			
R	#	$\bar{a}$	$\hat{\mathbf{V}}$	R	#	$\bar{a}$	$\hat{\mathbf{V}}$	R	#	$\bar{a}$	$\hat{\mathbf{V}}$	R	#	$\bar{a}$	$\hat{\mathbf{V}}$	R	#	$\bar{a}$	$\hat{\mathbf{V}}$
(a) *Sample 06*																			
Tot	619	0.951	− 5.866	Tot	234	0.372	− 5.234	Tot	183	0.768	− 4.271	Tot	431	0.551	1.501	Tot	162	0.387	5.759
> 6	15	0.994	− 6.502	3 to 4	25	0.975	− 0.137	> 5	6	0.989	− 5.688	> 3	43	0.932	− 1.854	2 to 3	26	0.782	4.772
5 to 6	35	0.996	− 6.008	2.5 to 3	38	0.612	− 3.752	4 to 5	10	0.981	− 5.595	2.5 to 3	72	0.861	− 0.078	2.5 to 3	8	0.702	− 4.189
4 to 5	156	0.993	− 6.560	2 to 2.5	97	0.369	− 6.872	3 to 4	35	0.979	− 4.697	2 to 2.5	154	0.647	1.169	2 to 2.5	18	0.610	9.777
3 to 4	316	0.989	− 5.715	1.5 to 2	63	0.109	− 6.539	2 to 3	49	0.943	− 2.064	1.5 to 2	137	0.269	7.134	1.5 to 2	92	0.451	4.578
2.5 to 3	80	0.878	− 4.630					1.5 to 2	29	0.660	− 9.520	< 2	162	0.462	8.659	< 1.5	40	0.151	19.469
< 2.5	16	0.098	− 13.875					< 1.5	54	0.477	− 2.948								
(b) *Sample 03C*																			
Tot	298	0.985	− 7.963					Tot	120	0.976	− 8.428	Tot	112	0.493	− 6.014				
> 6	21	0.992	− 7.357					> 4	6	0.986	− 5.604	2 to 3	34	0.897	− 2.255				
5 to 6	39	0.995	− 7.762					3 to 4	39	0.991	− 7.545	1.5 to 2	35	0.468	− 17.463				
4 to 5	113	0.994	− 8.157					2.5 to 3	17	0.904	− 9.981	< 1.5	36	0.083	39.152				
3 to 4	130	0.977	− 7.586					2 to 2.5	24	0.995	− 8.505								
2.5 to 3	27	0.982	− 8.697					2 to 3	41	0.957	− 9.083								
< 2.5	32	0.981	− 9.261					< 2.5	34	0.982	− 9.181								

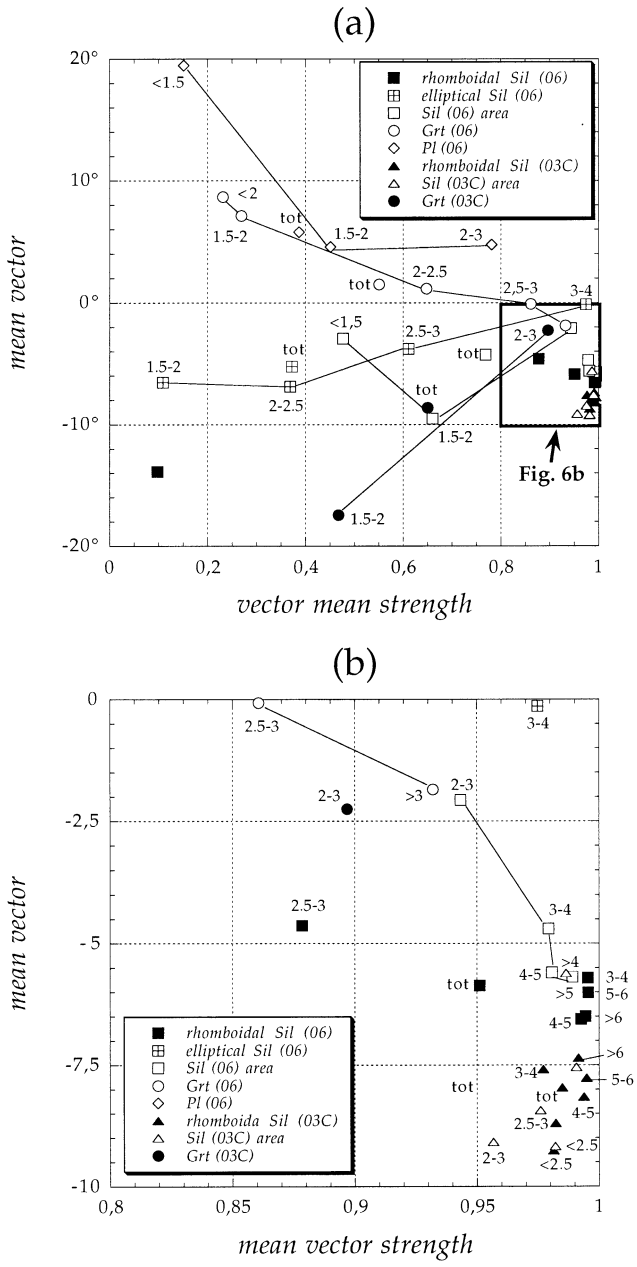

Fig. 6. (a) Values of $\hat{\mathbf{V}}$ plotted against $\bar{a}$ for θ measured for the best-fit ellipse (see Fig. 1), for different ranges in aspect ratio (range values given beside each symbol) and different minerals (connected by tie lines). Rhomboidal and elliptical *Sil* refer to isolated porphyroclasts in the matrix, whereas *Sil area* refers to the total porphyroclasts measured in small sample areas. (b) Enlargement of the solid rectangle outlined on (a).

even though individual clasts have seen very different shear strains, implies that the fabric is strain-insensitive and that, in order to develop such a high fabric intensity, the *Sil* orientation must be stable. This is further supported by the fact that a similar SPO is developed in both the studied samples and that the SPO of *Sil* is easily identified in all the mylonites (about a hundred samples). It is reasonable to assume that these samples, taken from different localities and different mylonitic shear zones, have accumulated significantly different bulk strains. This is independently

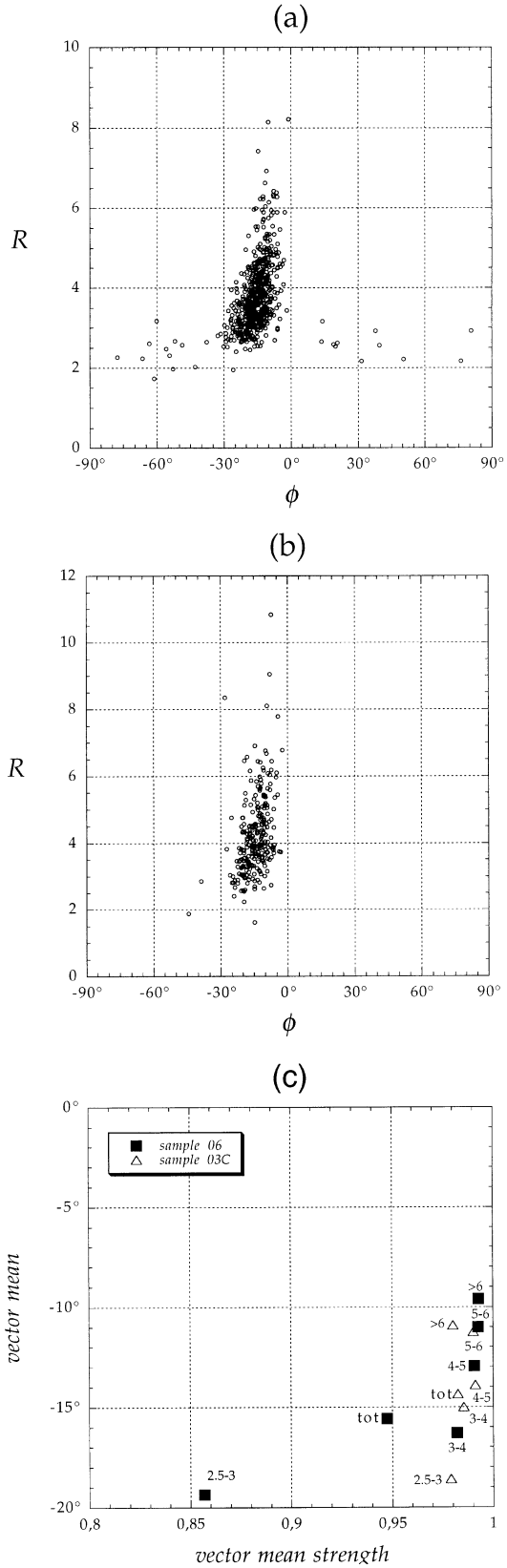

Fig. 7. Inclination ϕ of the long side of rhomboidal *Sil* (see Fig. 1) as a function of R for sample 06 (a) and 03C (b). The plot of $\hat{\mathbf{V}}$ plotted against $\bar{a}$ for ϕ is given as (c). Data listed in Table 3.

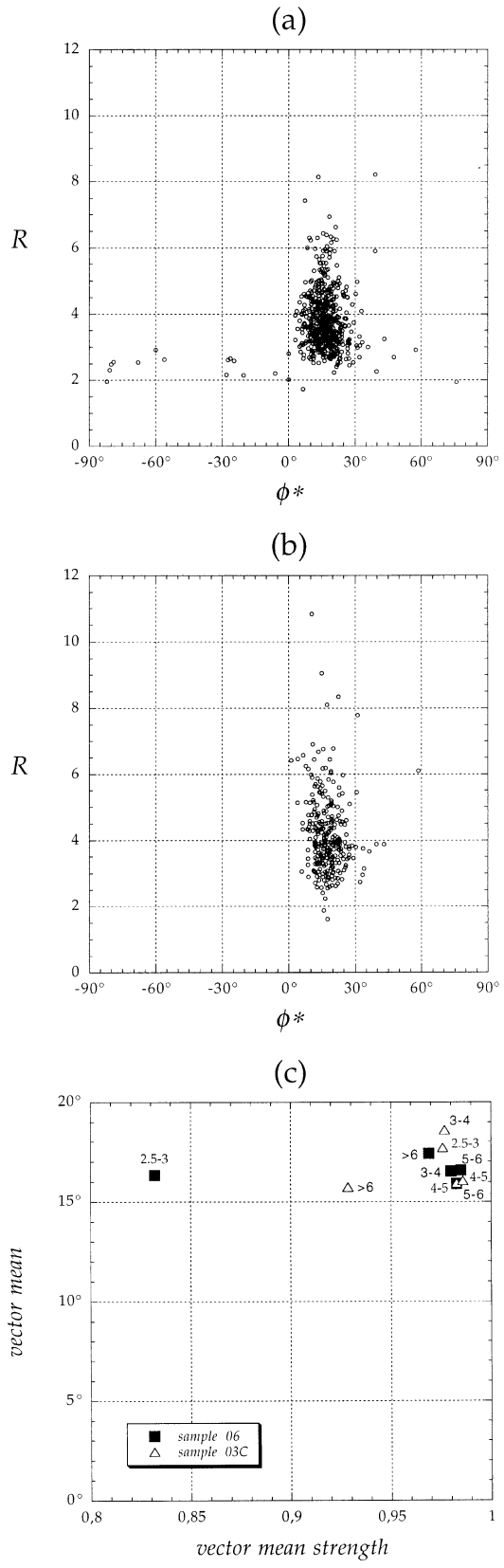

Fig. 8. Inclination ϕ^* of the short side of rhomboidal *Sil* (see Fig. 1) as a function of R for sample 06 (a) and 03C (b). The plot of $\hat{\mathbf{V}}$ plotted against $\bar{a}$ for ϕ is given as (c). Data listed in Table 4.

Table 3
$\hat{\mathbf{V}}$ against $\bar{a}$ for angle ϕ for the long side of rhomboidal *Sil* as a function of R in samples 06 and 03C

Sample 06				Sample 03C			
R	#	$\bar{a}$	$\hat{\mathbf{V}}$	R	#	$\bar{a}$	$\hat{\mathbf{V}}$
Tot	618	0.948	− 15.568	Tot	295	0.983	− 14.368
> 6	15	0.993	− 9.606	> 6	21	0.980	− 10.913
5 to 6	35	0.993	− 11.000	5 to 6	39	0.990	− 11.250
4 to 5	156	0.991	− 12.959	4 to 5	76	0.991	− 13.895
3 to 4	318	0.982	− 16.285	3 to 4	129	0.986	− 14.993
2.5 to 3	80	0.857	− 19.363	2.5 to 3	26	0.979	− 18.595

Table 4
$\hat{\mathbf{V}}$ against $\bar{a}$ for angle ϕ^* for the short side of rhomboidal *Sil* as a function of R in samples 06 and 03C

Sample 06				Sample 03C			
R	#	$\bar{a}$	$\hat{\mathbf{V}}$	R	#	$\bar{a}$	$\hat{\mathbf{V}}$
> 6	15	0.969	17.418	> 6	21	0.929	15.736
5 to 6	35	0.985	16.567	5 to 6	39	0.983	15.940
4 to 5	156	0.983	15.898	4 to 5	76	0.986	16.057
3 to 4	318	0.980	16.528	3 to 4	130	0.977	18.590
> 3	524	0.981	16.368	> 3	266	0.975	17.255
2.5 to 3	80	0.832	16.328	2.5 to 3	27	0.976	17.703

suggested by the different degree of fabric evolution present in the different mylonites. In the case of the samples considered here, these different characteristics suggest a higher bulk strain in sample 06 than in sample 03C. Sample 06 shows a lower density of clasts (i.e. more advanced clast refinement), and values of mean and maximum aspect ratio of porphyroclasts that are also lower. It should be emphasised that variations in microstructure suggest the occurrence of strain gradients even within the same sample or thin section.

A strain-telescoped fabric, oriented close to the shear plane, is also present for low aspect ratio particles, but a strain-insensitive character is not as evident as for the more elongated particles. These weaker, low-aspect-ratio fabrics may be better explained by existing models for the development of SPO, suggesting that a fundamental change in mechanism occurs above a critical aspect ratio.

8.2. Comparison with experimental and theoretical data

A striking feature of MM mylonites is the near parallelism of elongated porphyroclasts with aspect ratio $R < 3$. The SPO is stronger in sample 03C (with pervasive ECC), where a high intensity fabric is also developed for particles with $R < 3$. The SPO is similar for both elliptical and rhomboidal porphyroclasts and, therefore, is apparently independent of porphyroclast shape. This is in agreement with analogue scale-model experiments, which have

established that the exact shape has only a minor influence on rotational properties and that the kinematic behaviour closely follows that of the best fit ellipse enveloping the particle (e.g. see Fig. 1; Arbaret et al., 2001).

Thin sections orthogonal and parallel to the mylonitic lineation establish that *Sil* is approximately axisymmetric, with the long axis lying in a plane orthogonal to the foliation and containing the lineation (*XZ* plane). Therefore, a comparison with 2D theoretical models is appropriate.

The SPO present in elongated porphyroclasts ($R > 3$) is considered first and compared with the models categorised in Table 1. The strain-insensitive, strain-telescoped fabric of elongated porphyroclasts in MM mylonites, as established above, is not consistent with Model 1. This model considers the evolution of an initially random population that remains unchanged during deformation, with no interactions between objects or any grain size refinement process. It predicts that the fabric is transient and continuously oscillating. Even if the argument about strain insensitivity is ignored, Model 1 cannot explain the SPO in the MM mylonites. In simple shear, elongated porphyroclasts can stay close to the shear plane over a relatively large γ range owing to the slow rotation rates in that orientation, but porphyroclasts with different aspect ratio should have different mean vectors and mean vector intensities for any specific γ value.

A strong, strain-insensitive transverse SPO in mylonites could be developed during general non-coaxial bulk deformation (Model 2). This model could also account for the observed 'bimodal' fabric: particles with aspect ratios above a critical value should approach a stable position while those below this critical value should continue to rotate. In a thinning shear zone, however, the predicted stable positions (Model 2a) are inclined to the shear plane in the opposite sense to that observed in the studied mylonites. The observed SPO would be consistent with a thickening shear zone (Model 2b). In both Models 2a and 2b, however, there should be a dependence of the attitude of the SPO on the *R* value, in contrast to our data.

If we take into consideration the experimental results, particle interaction may cause a significant deviation from the theoretical behaviour of isolated particles and could produce a transverse steady-state fabric with the same orientation as observed in the studied mylonites (Models 4 and 5). In the MM mylonites, interaction is important. This is shown by the common occurrence of tiling features, attributable to both the relatively high density of porphyroclasts and the high finite strain. The fabric intensity measured in experiments involving interfering objects is always lower than that expected for non-interfering objects, however, in contrast to the very high fabric intensity measured in the MM mylonites. In addition, the tiling effects observed in the experiments do not occur in MM mylonites, where interfering particles apparently do not rotate. Similar considerations apply to the case where some slip occurs at the particle–matrix interface, which should lead to relatively low intensity fabrics (Model 7). In the analysis of Tikoff and Teyssier (1994), the Jeffery model produces low intensity fabrics similar to Models 4 and 5 and cannot, therefore, explain the observed high intensity fabric in the MM mylonites. The two March models predict fabrics consistent with that in the MM mylonites (i.e. a low angle, high intensity SPO with the same antithetic asymmetry), but March's theory was developed for infinitely long particles and is not a good mechanical description of the rotational behaviour of particles with moderate aspect ratios.

Model 8 of Cladouhos (1999b) does predict an oblique SPO similar to that of porphyroclasts in the MM mylonites. This model is purely kinematic. It could just as well apply to mylonites as to brittle rocks, provided there is comparable anisotropic behaviour with preferred shear along specific shear surfaces (potentially the mylonitic foliation and the ECC in the MM mylonites). In the model of Cladouhos (1999b), however, only the particulate flow step of the deformation path is considered to contribute to development of SPO. The SPO in this step is calculated following Ghosh and Ramberg (1976) and, therefore, shows the same characteristics as discussed for Model 2 above.

In MM mylonites, the SPO of porphyroclasts with an aspect ratio lower than three have a mean orientation close the shear plane. In this case, the orientation data are consistent with the standard theoretical models based on the Jeffery theory. The numerical calculations of Cladouhos (1999a), adopting Model 1, indicate that a random initial population of porphyroclasts with aspect ratios in the range of 1.4–2.8 (plus 10% grains > 3) and average axial ratio of 1.9 can develop a bulk SPO close to the shear plane for a simple shear strain of just four. The fabric is oscillating both in intensity and orientation, but for $\gamma > 10$, the mean vector remains within $\pm 15°$ of the shear plane, with the fabric intensity varying from random to moderate ($\bar{a} < 0.5$). This is in good accord with the measured SPO of low aspect ratio porphyroclasts in MM mylonites. The analysis of Cladouhos, however, refers to constant shape, non-interacting porphyroclasts that accumulated the same total strain. This is not the case in the MM mylonites, where microstructures indicate a continuous, episodic supply of new porphyroclasts by fracturing and grain size refinement and, hence, a strain-telescoped fabric. This possibility is taken into consideration in Model 3, developed for magmatic rocks, but also potentially applicable to many mylonites. In Model 3, the SPO has a low-intensity fabric oriented close to the shear plane and can well explain the SPO of the low aspect ratio particles in the studied mylonites. Given the high strain accumulated in mylonites and the relatively high density of porphyroclasts, particle interaction may also play a significant part in the development of SPO. Factorisation of the measured SPO into the above components (Models 1, 3 and 4–5) is not possible at this stage, however, and would require a very large data set.

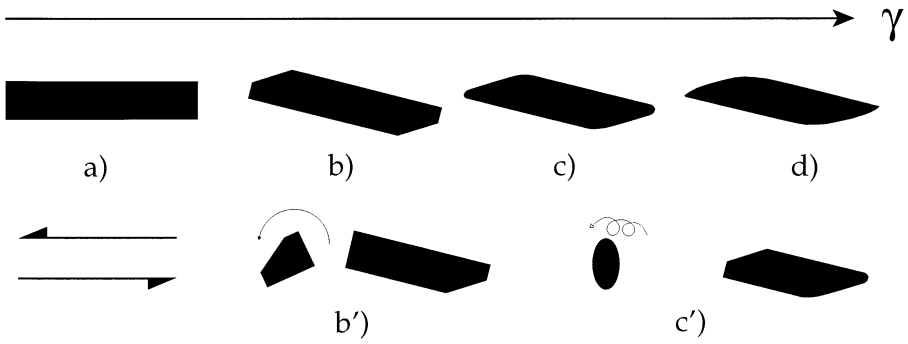

Fig. 9. Progressive development of different *Sil* shapes by grain size refinement with increasing shear strain (a–d), from an initial rectangular microboudin of prismatic *Sil* to the final sigmoidal shape. The different shapes reported here are developed by progressive pressure solution along ECC tangential to the short sides of the porphyroclasts. Intermediate shapes (b) include a relict portion of short rectangular sides (see also Fig. 4b). Fracturing during this refinement process (b′, see Fig. 4c and d) can produce lower-aspect ratio clasts that rotate and acquire an elliptical shape during several cycles of rotation (c′, see Fig. 3d).

8.3. Origin of the different shapes and aspect ratio of porphyroclasts

Experiments show that equant and elongated objects embedded in a matrix flowing in simple shear may evolve into elliptical or circular equilibrium shapes (in cross-section) with increasing shear strain by combined rotation and recrystallisation at points of stress concentration (ten Brink and Passchier, 1995). Progressive smoothing of irregularities results in a decrease in recrystallisation rates and allows the porphyroclast to maintain its shape with increasing strain and further rotation. In MM mylonites, the circular/elliptical shape of porphyroclasts with low aspect ratio ($R < 3$) is probably attributable to the above mechanism. That they have rotated is demonstrated by δ-shaped tails and the low fabric intensity. The ellipticity of these porphyroclasts is inherited from the initial aspect ratio of clasts and depends on the fracturing mode.

The rhomboidal shape of *Sil* is also acquired during deformation. The progressive development of the different *Sil* shapes with increasing γ is sketched in Fig. 9. Initial *Sil* microboudins are rectangular and acquire a stable position inclined to the mylonitic foliation. During the subsequent strain history, these immobilised porphyroclasts change their shape to a rhomboidal form, with intermediate shapes showing relict segments of rectangular faces. This intermediate shape cannot be explained by crystal plastic deformation of *Sil*, for which there is no microstructural evidence. There is also no evidence for abrasion. Rather, the change in shape appears to be the result of dissolution and/or reaction of the immobilised porphyroclast against ECC planes. Such an origin is strongly supported by the fact that the short sides of rhomboidal *Sil* porphyroclast have a constant orientation parallel to ECC, independent of the porphyroclast aspect ratio. Porphyroclasts at any stage of their shape development may undergo fracturing/microboudinage. The resulting clasts also establish stable positions if they have $R > 3$ (or even a lower value in the presence of a pervasive ECC) or start to rotate if they are more equant (Fig. 4c and d). Rotating fragments give rise to elliptical porphyroclasts after cycles of rotation. All these stages of porphyroclast evolution are well preserved in the mylonites.

8.4. A possible role of ECC on stabilisation of elongated objects

The orientation of *Sil* in MM mylonites closely resembles that of asymmetric pull-aparts, especially the type 2b pull-aparts of Hanmer (1986), and common mica-fish in mylonites (Lister and Snoke, 1984). The main differences between the *Sil* porphyroclasts and Hanmer's (1986) type 2b pull-aparts are that: (1) *Sil* porphyroclasts are rigid objects and the competence contrast with the matrix is high, whereas Hanmer's pull-aparts are developed in pinch-and-swell boudinage structures; and (2) *Sil* porphyroclasts are isolated and are not influenced by the distortional field of adjacent boudins. In comparison with common mica-fish, *Sil* porphyroclasts are rigid objects and their shape consists of faces tangential to ECC rather than to C surfaces (Lister and Snoke, 1984). As a result, the asymmetry in monoclinic shape relative to the shear sense is the opposite.

In Hanmer's (1986) model, the SPO of pull-aparts, stair-stepping to the shear plane, is explained by antithetic rotation owing to the development of a pair of ECC. Even in the absence of compositional heterogeneities, this effect is well documented in strongly anisotropic rocks (Platt and Vissers, 1980). Slip along internal anisotropy of pull-aparts and local deviation from simple shear, caused by slight deviation of the anisotropy from the shear plane, is considered important for the development of type 2 pull-aparts and in particular for type 2a ones. The contributions of the two slip directions, along ECC and internal anisotropy, are synthetic and mutually additive and must be coeval to achieve an imposed general 2D strain (similar to the so-called Von Mises criterion in crystal plasticity; e.g. Mancktelow, 1987; Cladouhos, 1999b).

As discussed above, dissolution along ECC may be instrumental in developing the observed rhomboidal shapes and slip along ECC appears to be an essential deformation

mode in MM mylonites. In all samples, the short sides of *Sil* are very well aligned and individual ECC planes are developed along and perfectly parallel to *b* faces. The shape evolution of Sil porphyroclasts suggests that ECC develops continuously during deformation and is not simply a late-stage structure, as observed in other mylonites (e.g. Passchier, 1991). A further constraint on the interpretation of SPO is the stable orientation of elongated *Sil*. These porphyroclasts rapidly attain stable positions, as witnessed by the strong fabric intensity, despite continuous disturbance by porphyroclast interactions and grain refinement processes. Another observation is that the aspect ratio influences the inclination of the *a* faces of elongated *Sil* rhomboids, with ϕ decreasing with increasing *R*. In contrast, the *b* faces, tangential to the ECC, are fixed in orientation.

Given the above constraints, an intuitive kinematic model could explain aspects of the stable orientation of *Sil*. Close to the porphyroclast/matrix interface, interface–parallel shear along *b* faces induces an orthogonal (to the bulk shear plane) displacement component of flow (of magnitude $b \sin \phi^*$). To maintain strain compatibility with surrounding domains of undisturbed matrix laminar flow, an equivalent opposite orthogonal component (of magnitude $a \sin \phi$) must be recovered through interface–parallel shear along *a* faces. The angle ϕ^* is approximately constant, being fixed by the ECC orientation. Therefore, to maintain equilibrium in the local orthogonal displacement components, an increase in the porphyroclast aspect ratio (also resulting in an increase of a/b) requires a decrease in the angle ϕ. This is consistent with the observed dependence of ϕ on *R*. This simple model, however, cannot account for other characteristics of the SPO such as the stair-stepping geometry of porphyroclast tips.

9. Conclusions

The SPO of elongated porphyroclasts measured in the MM mylonites is not well explained by any current analytical or experimental model. The measurements establish that rigid porphyroclasts with $R > \sim 3$ attain a stable orientation. The characteristic rhomboidal *Sil* shape and intimate spatial relationship of the well-aligned short sides to ECC suggest that ECC may play a critical role in stabilisation of elongate rigid particles. The discrepancy between observation and the existing models suggests that the relatively simple assumptions of these models (homogeneous, isotropic, linear viscous matrix with a coherent matrix/particle interface) may not be appropriate for all highly sheared rocks.

Acknowledgements

This research forms part of a project on multidisciplinary study of mylonites financed by the University of Padova and this support is gratefully acknowledged. Thorough and constructive reviews by T. Cladouhos and P. Bons helped improve the original manuscript. Image analysis was performed using the public domain NIH Image program (developed at the US National Institutes of Health and available on the Internet at http://rsb.info.nih.gov/nih-image/).

References

Agterberg, F.P., 1974. Geomathematics: Mathematical Background and Geoscience Applications. Elsevier Science, Amsterdam 596pp.

Arbaret, L., Diot, H., Bouchez, J.-L., 1996. Shape fabrics of particles in low concentration suspensions: 2D analogue experiments and application to tiling in magma. Journal of Structural Geology 18, 941–950.

Arbaret, L., Mancktelow, N., Burg, J.-P., 2001. Effect of shape and orientation on rigid particle rotation and matrix deformation in simple shear flow. Journal of Structural Geology 23, 113–115.

Benn, K., Allard, B., 1989. Preferred mineral orientations related to magmatic flow in ophiolite layered gabbros. Journal of Petrology 30, 925–946.

Bons, P.D., Barr, T.D., ten Brink, C.E., 1997. The development of δ-clasts in non-linear viscous materials: a numerical approach. Tectonophysics 270, 29–41.

Cladouhos, T.T., 1999a. Shape preferred orientations of survivor grains in fault gouge. Journal of Structural Geology 21, 419–436.

Cladouhos, T.T., 1999b. A kinematic model for deformation within brittle shear zones. Journal of Structural Geology 21, 437–448.

Debat, P., Sirieys, P., Deramond, J., Soula, J.C., 1975. Paleodéformations d'un massif orthogneissique (massif des Cammazes, Montagne Noire Occidentale, France). Tectonophysics 28, 159–183.

Ferguson, C.C., 1979. Rotations of elongate rigid particles in slow non-Newtonian flows. Tectonophysics 60, 247–262.

Fernandez, A., 1988. Strain analysis from shape preferred orientation in magmatic flow. Bulletin of the Geological Institut of the University of Uppsala 14, 61–67.

Fernandez, A., Febesse, J.L., Mezure, J.F., 1983. Theoretical and experimental study of fabrics developed by different shaped markers in two-dimensional simple shear. Bulletin de la Societé Géologique de France 7, 319–326.

Freeman, B., 1985. The motion of rigid ellipsoidal particles in slow flows. Tectonophysics 113, 163–183.

Gay, N.C., 1968. The motion of rigid particles embedded in a viscous fluid during pure shear deformation of the fluid. Tectonophysics 5, 81–88.

Ghosh, S.K., Ramberg, H., 1976. Reorientation of inclusions by combination of pure shear and simple shear. Tectonophysics 34, 1–70.

Hanmer, S., 1986. Asymmetrical pull-aparts and foliation fish as kinematic indicators. Journal of Structural Geology 8, 111–122.

Hanmer, S., 1990. Natural rotated inclusions in non-ideal shear. Tectonophysics 176, 245–255.

Hinch, E.J., Leal, L.G., 1979. Rotation of small non-axisymmetric particles in a simple shear flow. Journal of Fluid Mechanics 92, 591–608.

Ildefonse, B., Launeau, P., Fernandez, A., Bouchez, J.L., 1992a. Effect of mechanical interactions on development of shape preferred orientations: a two-dimensional experimental approach. Journal of Structural Geology 14, 73–83.

Ildefonse, B., Sokoutis, D., Mancktelow, N.S., 1992b. Mechanical interactions between rigid particles in a deforming ductile matrix. Analogue experiments in simple shear flow. Journal of Structural Geology 14, 1253–1266.

Ildefonse, B., Mancktelow, N.S., 1993. Deformation around rigid particles: the influence of slip at the particle/matrix interface. Tectonophysics 221, 345–359.

Jeffery, G.B., 1922. The motion of ellipsoidal particles immersed in a

viscous fluid. Proceedings of the Royal Society of London A 102, 161–179.

Ježek, J., Melka, R., Schulmann, K., Venera, Z., 1994. The behaviour of rigid triaxial particles in viscous flows—modelling of fabric evolution in a multiparticle system. Tectonophysics 229, 165–180.

Lister, G.S., Snoke, A.W., 1984. S–C mylonites. Journal of Structural Geology 6, 617–638.

Luneau, P., Cruden, A.R., 1998. Magmatic fabric acquisition mechanisms in a syenite: results of a combined anisotropy of magnetic susceptibility and image analysis study. Journal of Geophysical Research 103, 5067–5089.

Mancktelow, N.S., 1987. Quartz textures from the Simplon Fault Zone, southwest Switzerland and north Italy. Tectonophysics 135, 133–153.

March, A., 1932. Mathematische Theorie der Regelung nach der Korngestalt bei affiner Deformation. Zeitschrift für Kristallographie, Mineralogie und Petrographie 81, 285–297.

Mason, S.G., Manley, R.S., 1957. Particle motion in sheared suspension: orientations and interactions of rigid rods. Proceedings of the Royal Society of London 238, 117–131.

Masuda, T., Shibutani, T., Kuriyama, M., Igarashi, T., 1990. Development of microboudinage: an estimate of changing differential stress with increasing strain. Tectonophysics 178, 379–387.

Masuda, T., Michibayashi, K., Otha, H., 1995. Shape preferred orientation of rigid particles in a viscous matrix: re-evaluation to determine kinematic parameters of ductile deformation. Journal of Structural Geology 17, 115–129.

Passchier, C.W., 1987. Stable positions of rigid objects in non-coaxial flow—a study in vorticity analysis. Journal of Structural Geology 9, 679–690.

Passchier, C.W., 1991. Geometric constraints on the development of shear bands in rocks. Geologie en Mijnbouw 70, 203–211.

Passchier, C.W., Sokoutis, D., 1993. Experimental modelling of mantled porphyroclasts. Journal of Structural Geology 15, 895–909.

Passchier, C.W., Trouw, R.A.J., 1996. Microtectonics. Springer-Verlag, Berlin, 289pp.

Passchier, C.W., ten Brink, C.E., Bons, P.D., Sokoutis, D., 1993. δ objects as a gauge for stress sensitivity of strain rate in mylonites. Earth and Planetary Science Letters 120, 239–245.

Pennacchioni, G., Cesare, B., 1997. Ductile-brittle transition in pre-Alpine amphibolite facies mylonites during evolution from water-present to water-deficient conditions (Mont Mary nappe, Italian Western Alps). Journal of Metamorphic Geology 15, 777–791.

Pennacchioni, G., Fasolo, L., Morandi Cecchi, M., Salasnich, L., 2000. Finite-element modelling of simple shear flow in Newtonian and non-Newtonian fluids around a circular rigid particle. Journal of Structural Geology 22, 683–692.

Platt, J.P., Vissers, R., 1980. Extensional structures in anisotropic rocks. Journal of Structural Geology 2, 397–410.

Ramsay, J.G., Huber, M., 1987. The Techniques of Modern Structural Geology. Volume 1: Strain Analysis. Academic Press, London.

Reed, L.J., Tryggvason, E., 1974. Preferred orientations of rigid particles in a viscous matrix deformed by pure shear and simple shear. Tectonophysics 24, 85–98.

Robertson, C.R., Acrivos, A., 1970. Low Reynolds number shear flow past a rotating circular cylinder. Part 1: Momentum transfer. Journal of Fluid Mechanics 40, 685–704.

Shelley, D., 1995. Asymmetric shape preferred orientations as shear-sense indicators. Journal of Structural Geology 17, 509–517.

ten Brink, C.E., 1996. Development of Porphyroclast Geometries during Non-coaxial Flow. Geologica Ultraiectina 142, 163pp.

ten Brink, C.E., Passchier, C.W., 1995. Modelling of mantled porphyroclasts using non-Newtonian rock analogue materials. Journal of Structural Geology 17, 131–146.

Tikoff, B., Teyssier, C., 1994. Strain and fabric analyses based on porphyroclast interaction. Journal of Structural Geology 16, 477–491.

Tullis, T.E., 1976. Experiments on the origin of slaty cleavage and schistosity. Geological Society of America Bulletin 87, 745–753.

Willis, D.G., 1977. A kinematic model of preferred orientation. Geological Society of America Bulletin 88, 883–894.